Full Length Article

Detonation properties and nitrogen oxide production in ammonia–hydrogen–air mixtures

Fernando Veiga-López [a],*, Rémy Mével [b]

[a] *Aerolab, Research Institute of Physics and Aerospace Science, University of Vigo, Campus de Ourense, Ourense, 32004, Galicia, Spain*
[b] *Center for Combustion and Energy, School of Vehicle and Mobility, Tsinghua University, China*

ARTICLE INFO

ABSTRACT

Ammonia is a promising compound for chemical storage of renewable energy produced from non-continuous sources. However, the low reactivity of ammonia requires to use ammonia–hydrogen blends as a fuel for combustion applications. The present study corresponds to a first numerical assessment of the potential of ammonia–hydrogen–air mixtures as reactive mixtures for detonation engine applications. Both ideal and curved detonation models were employed to calculate the detonation properties, entropy production, and NOx production for mixtures with varying amounts of ammonia and hydrogen under a wide range of initial thermodynamics conditions. Interestingly, our calculations show that the entropy production and the amount of nitrogen oxides produced at the Chapman–Jouguet state respectively decreases and increases with the proportion of hydrogen in the ammonia–hydrogen blend. These aspects could have a great impact on engine efficiency and air pollution and should be considered with care. Our results also demonstrate that only mixtures with relatively low amounts of ammonia, i.e., X_{NH3} lower than 0.25 of the fuel blend, can be employed for detonation engine applications.

1. Introduction

Humanity is currently facing an environmental and an energy crises, which are related to the continuous use of fossil fuels combustion as the main source of primary energy [1]. To address these issues, it is required to employ renewable energy sources and achieve net-zero carbon emission in the next decades. Following hydraulic-driven turbine, the two main techniques to harvest renewable energy correspond to wind turbine and solar panel. Despite their interesting performances in producing clean energy, these two technologies present the tremendous drawback of being discontinuous. This drawback can potentially be overcome by chemically storing energy produced during periods of high production. Two interesting species to achieve efficient chemical storage are hydrogen and ammonia [2,3]. Both fuels present a number of advantages and drawbacks. While the production of hydrogen is less expensive than the production of ammonia, storage and transportation, especially over very long distances, makes ammonia a more cost effective energy carrier [2]. Ammonia is also more compatible with the existing infrastructure than hydrogen, since it presents physical properties close to those of liquefied petroleum gas [2]. For hydrogen, existing infrastructures, such as natural gas transportation pipelines, permit to add only few percent of hydrogen to natural gas, which limits the decarbonation potential of hydrogen. The high reactivity of hydrogen

makes it an appropriate fuel for combustion application, while such a property poses important safety issues. On the contrary, the combustion properties of ammonia, in particular its low reactivity [4], are rather unfavorable for combustion application. On the other hand, ammonia exhibits a very low potential for accidental combustion, and risks associated with its utilization are related to its toxicity. One alternative option to ensure ammonia can be employed for combustion application is to use blends of H_2 and NH_3, possibly formed through ammonia cracking. Nevertheless, it is not clear what hydrogen to ammonia ratio should be used to ensure appropriate combustion properties for practical applications.

In addition to efficient, renewable fuels, achieving net-zero carbon emission requires the utilization of efficient engines. One promising approach to obtain high thermodynamic efficiency and high thrust for propulsion applications is to employ engines that rely on detonation, such as the pulsed detonation engine (PDE), or the rotating detonation engine (RDE). A PDE is a semi-opened cylindrical tube. The ignition system is typically positioned at the closed end and the ejection of the burnt gas is taking place at the open end [5]. The operating cycle of a PDE is composed of the following phases: (i) Fuel and oxidizer are injected and mixed in the combustion chamber; (ii) Detonation initiation using a high-energy source or via the DDT process; (iii) Detonation

---

propagation; (iv) High-pressure gas fills the detonation chamber; (v) Detonation exits the chamber and air is drawn in due to the reduced pressure. Despite presenting the advantage of design simplicity, PDEs work on a discontinuous operation mode and the associated need for high-frequency repeated reactive mixture filling and detonation initiation complicate their practical applications [6]. As a consequence, recent efforts on detonation engine development have been focused on RDE [7,8]. A rotating detonation engine is based on a continuous detonation process and is designed according to an annular geometry which enables to confine the rotating detonation wave. The fuel-oxidant mixture is continuously injected from the injection wall and forms a layer of reactive gas which is consumed by a detonation. The height of the detonation is controlled by the height of the reactive layer. Above the detonation propagating at a reactive/non-reactive interface, an oblique shock wave is formed and propagates alongside the detonation. The expansion of the burnt gas provide impulse [9]. As compared to a PDE, the RDE presents the advantage of a higher simplicity since only the injection part needs to be optimized to achieve good performances. Nevertheless, a number of non-idealities can significantly affect the performances of an RDE. According to Raman et al. [10], these non-idealities include: (i) secondary combustion, either in front of the detonation wave, i.e., parasitic combustion, or behind the detonation wave, i.e., commensal combustion; (ii) inhomogeneous mixing of the reactants; and (iii) multiple competing waves. Regardless of the extend of these non-idealities, the semi-confined configuration of the detonation wave in an RDE induces the continuous interaction of the front with an inert layer, deforming and curving the detonation front, and thus modifying its propagation speed and characteristics. In case the layer height is too low, detonation failure would occur [11,12].

While hydrogen detonation have been extensively studied [13–18], detonation in ammonia-based mixtures have been largely underexplored. Akbar et al. [19] performed a limited number of cell width measurements for different mixtures containing ammonia. They showed that ammonia acts as a detonation inhibitor. Vasil'ev and Vasiliev [20] investigated the detonation structure in NH_3–O_2, NH_3-air, and NH_3–N_2O mixtures. They reported that a single cellular structure was observed in NH_3–O_2, whereas a dual-sized structure was obtained for NH_3–N_2O. Weng et al. [4] characterized the detonation sensitivity of ammonia-oxygen and ammonia-nitrous oxide mixtures. They provided a comparison with other commonly studied fuels and showed that ammonia is rather insensitive to detonation, even more so that methane. Yu and Zhang [21] numerically studied end-gas auto-ignition in hydrogen–ammonia–air mixtures contained in a closed vessel. Three outcomes could be observed: (i) simple flame propagation; (ii) auto-ignition; and (iii) detonation onset. It is interesting to note that detonation formation was observed only for a hydrogen to total fuel content equal to or higher than 0.3. Zhu et al. [22] investigated the stability behavior of unsteady one-dimensional (1D) detonation in hydrogen–ammonia–air mixtures. The detonations were initiated by a hot spot located at one end of the linear computational domain. It was shown that a higher hydrogen content tends to stabilize the detonation, suppressing the pulsating behavior. For a given hydrogen content of 20% in the fuel, a pulsating behavior was observed for equivalence ratio in the range 0.6–2.5. Kohama et al. [23] performed two-dimensional (2D) numerical simulations of detonation propagating in hydrogen–ammonia–air mixtures using detailed chemistry. It was shown that the regularity of the cellular structure increases with the fraction of hydrogen in the mixture. For large ammonia contents, transverse detonation with sub-structures were observed.

Therefore, the objectives of this work are two-fold: (i) to study the detonation properties of hydrogen–ammonia blends under ideal detonation conditions; and (ii) to investigate quasi-steady, weakly curved hydrogen–ammonia detonations, aiming to provide a first assessment on the soundness of this fuel blend for PDE/RDE applications. The remainder of the document is structured as follows. Section 2 introduces the physical and chemical models used for the analysis of detonations. Next, Section 3 includes all the results obtained for both ideal and curved detonations and the corresponding discussions. Finally, Section 4 summarizes the main findings of the work.

2. Physical and chemical models

2.1. Detonation models

Neglecting diffusion, heat transfer, viscosity, body force, and the cellular structure, a one-dimensional (1D) steady or quasi-steady detonation wave in an ideal gas can be described by the following set of governing equations

$$\frac{d\rho}{dt} = -\rho \frac{\dot{\sigma} - wM^2\alpha}{\eta}, \tag{1a}$$

$$\frac{dp}{dt} = -\rho w \frac{dw}{dt}, \tag{1b}$$

$$\frac{dw}{dt} = w \frac{\dot{\sigma} - w\alpha}{\eta}, \tag{1c}$$

$$\frac{dY_i}{dt} = \frac{W_i\dot{\omega}_i}{\rho}. \tag{1d}$$

where ρ is the density, t is time, w is the flow velocity, η is the sonic parameter given by $\eta = 1 - M^2$ where $M = w/a_f$ is the Mach number with respect to the detonation front and a_f is the frozen speed of sound, p is the pressure, Y_i, W_i and $\dot{\omega}_i$ are respectively the mass fraction, molecular weight and source term of species i. The symbol $\dot{\sigma}$ represents the thermicity given by

$$\dot{\sigma} = \sum_{i=1}^{N} \left(\frac{\overline{W}}{W_i} - \frac{h_i}{c_p T} \right) \frac{dY_i}{dt}, \tag{2}$$

where $\overline{W}$ is the mean molar mass, c_p is the constant-pressure specific heat, and h_i is the specific enthalpy of the ith species. The axial area change is defined by α and is related to the curvature κ as [24]
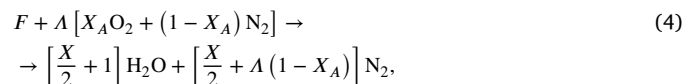
$$\alpha = \frac{1}{A}\frac{dA}{dx} = \kappa \left(\frac{D}{w} - 1 \right), \tag{3}$$

where A is the area, x is the spatial coordinate, $\kappa = 2/R_c$ for a spherical wave, R_c is the detonation radius, D is the detonation velocity.

As discussed in [24–26], the quasi-steady approach is applicable if (1) the characteristic chemical length-scale is much smaller than the detonation wave radius, and (2) the characteristic chemical time-scale is much shorter than the characteristic time-scale describing the variation of the detonation front velocity. Setting α to zero, the classical Zeldovich–von Neumann, Doering (ZND) model for steady planar detonation is recovered, which is also applied for part of the analysis.

Low-order physical models including curvature effects were found valuable in the past to predict limiting behaviors [27,28]. Namely, extensions to the ZND model including curvature losses yield the locus of steady-state solutions in detonation velocity (D) - curvature (κ) space; the so-called $D-\kappa$ curves. The existence of a maximum curvature, κ_{crit}, in these curves is a sign that this type of low-order models may provide meaningful estimates for detonability limits. Indeed these tools have been used extensively in theoretical studies [24,29–31] and have shown to be in agreement with experimental data [32–34].

To characterize the composition of the fresh gases, we used the stoichiometry of the global reaction as proposed by Fernández-Tarrazo et al. [35]:

$$F + \Lambda \left[X_A O_2 + (1 - X_A) N_2 \right] \rightarrow \tag{4}$$

$$\rightarrow \left[\frac{X}{2} + 1 \right] H_2O + \left[\frac{X}{2} + \Lambda (1 - X_A) \right] N_2,$$

with $\Lambda = (X + 2)/(4X_A)$ the number of moles of air that react with one mole of fuel. The fuel is composed of ammonia and hydrogen with respective mole fractions of X and $1 - X$; air is formed of O_2, with a mole fraction of $X_A = 0.21$ and of N_2, with a mole fraction of $1 - X_A$. Therefore, the equivalence ratio of the mixture is determined by

$$\phi = \frac{\left[X_F / (1 - X_F) \right] (X + 2)}{4X_A} \tag{5}$$

with X_F the molar fraction of fuel blend in the fresh mixture. Thus, the initial composition is given by:

$$X_{H_2} = \frac{1 - X}{1 + \Lambda/\phi},$$

$$X_{\mathrm{NH}_3} = \frac{X}{1 + \Lambda/\phi},$$

$$X_{\mathrm{O}_2} = \frac{X_A \Lambda}{\Lambda + \phi},$$

$$X_{\mathrm{N}_2} = \frac{(1 - X_A)\,\Lambda}{\Lambda + \phi}.$$

Regarding the chemical mechanism, that of Otomo et al. [36] was selected for the current analysis, one of the most recent mechanism for ammonia and ammonia/hydrogen combustion. It includes 32 chemical species and 216 reactions and has been extensively validated.

3. Results and discussion

First, in Section 3.1, the ideal ZND model is employed to study the effect of adding ammonia to hydrogen–air mixtures. Next, in Section 3.3, the effect of curvature on the detonation characteristics is assessed. For the whole study, the initial conditions of the mixtures are $T_0 = 300$ K, $p_0 = 100$ kPa, and $\phi = 1$ if not indicated otherwise.

3.1. Ideal detonations

3.1.1. Detonation properties analysis

In this sub-section, we investigate the impact of initial pressure and temperature for mixtures with various amounts of ammonia. Our study provides a comprehensive cartography of the detonation properties of NH_3–H_2-air mixtures as well as some insights into the possibility of using such mixtures for propulsion applications. nevertheless, it should be kept in mind that for some specific conditions, successfully initiating a detonation could be very challenging and would require very large-scale facilities [37,38].
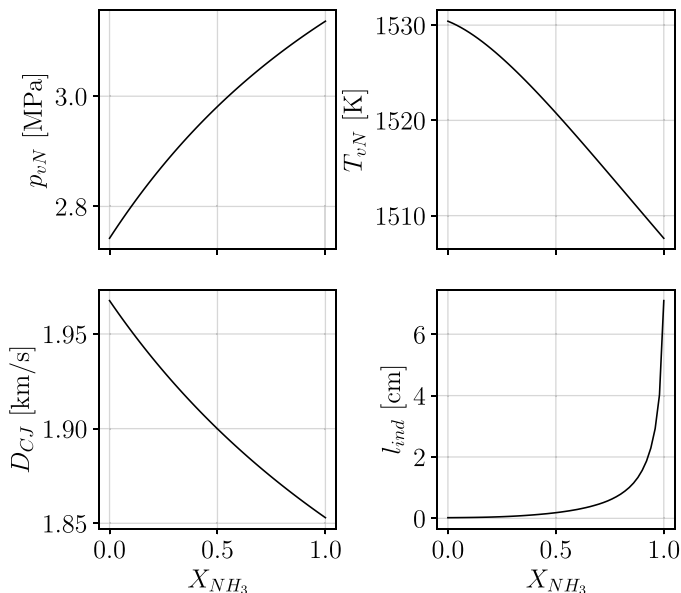

Fig. 1. Influence of NH_3 on detonation properties. Conditions: $p_0 = 100$ kPa, $T_0 = 300$ K, and $\phi = 1$.

3.2. Mixture composition and chemical model

Influence of mixture composition. Fig. 1 shows the variation of the detonation properties of interest with the addition of ammonia to hydrogen, from 0 to 100%. Including ammonia into the mixture slightly modifies the von Neumann (subscript vN) thermodynamic conditions, increasing (decreasing) p_{vN} (T_{vN}) by a maximum of 15% (1.3%). Likewise, NH_3 addition decreases both the ideal propagation speed D_{CJ} (5.7%) and chemical reaction rate. The latter provokes a sharp increase of the

induction length l_{ind}, defined as the distance between the shock and the peak thermicity, from around 7 mm up to 6.5 cm when large amounts of ammonia are included in the fuel blends (i.e., > 80% NH_3). Similar trends were reported for deflagrations [39,40], showing that ammonia slows down the chemistry and widens the reaction zone.
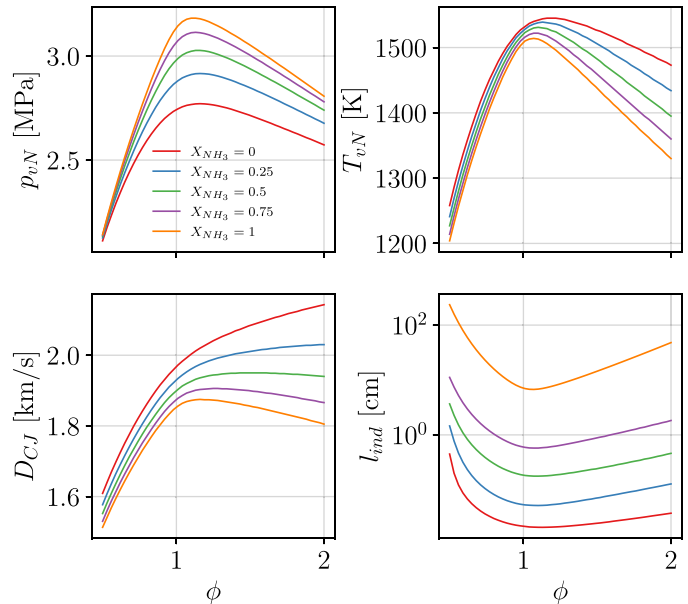

Fig. 2. Influence of equivalence ratio (ϕ) on detonation properties for different amounts of NH_3. Conditions: $p_0 = 100$ kPa and $T_0 = 300$ K.

In addition, Fig. 2 shows the influence of equivalence ratio, from slightly lean ($\phi = 0.8$) to rich ($\phi = 2$) conditions, on the main detonation properties, for selected amounts of ammonia in the fresh mixture. For p_{vN}, and T_{vN}, the evolutions with ϕ demonstrate asymmetric reverse U-shape with a maximum around the stoichiometry and steeper variations on the lean side than on the rich one. Increasing the amount of hydrogen essentially shifts the curves toward lower pressures and higher temperatures. Concerning the induction length, an opposite trend is found with asymmetric U-shaped curves, with a minimum around $\phi = 1$, and larger variations for lean mixtures. The induction length varies over order of magnitudes as the fuel composition changes from pure hydrogen to pure ammonia. As for the detonation velocity, a more complex evolution is observed and depends on the amount of ammonia. For high ammonia contents, the evolution is similar to the ones observed for p_{vN}. On the other hand, for large hydrogen contents, D_{CJ} continuously increases with equivalence ratio.

Influence of initial thermodynamic conditions. The influence of modifying the initial pressure p_0 of the mixture from 40 to 300 kPa is shown in Fig. 3 for different X_{NH_3} within the fuel blend. First, focusing our analysis on the constant mixture composition with $X_{\mathrm{NH}_3} = 0.25$ as an example, one observes that increasing p_0 increases both p_{vN} and T_{vN} from 1.5 MPa to 7.6 MPa and from 1480 K to 1550 K, respectively. Likewise, D_{CJ} (l_{ind}) increases (decreases) by 2.6% (by a factor of 5.7) for increasing values of p_0.

Modifying the fuel blend composition modifies the analyzed detonation parameters as well. First, the von Neumann thermodynamic conditions almost do not change at low initial pressures ($p_0 = 50$ kPa) when modifying X_{NH_3}; at $p_0 = 300$ kPa, p_{vN} shows a 5% increase and T_{vN} a decrease around 2% from pure H_2 to pure ammonia. Second, D_{CJ} (l_{ind}) continuously decreases (increases) for increasing X_{NH_3}, reporting slightly stronger (weaker) differences for lower p_0.

To complete the parametric analysis, the influence of the initial mixture temperature is reported in Fig. 4. For all compositions, i.e., for all contents of ammonia, the pressure (temperature) just behind the
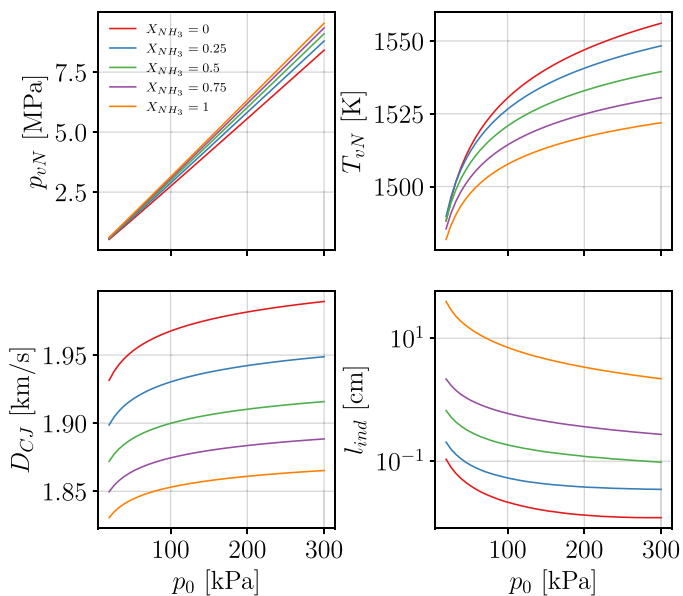
Fig. 3. Influence of initial pressure (p_0) on detonation properties for different amounts of NH$_3$. Conditions: $\phi = 1$ and $T_0 = 300$ K.
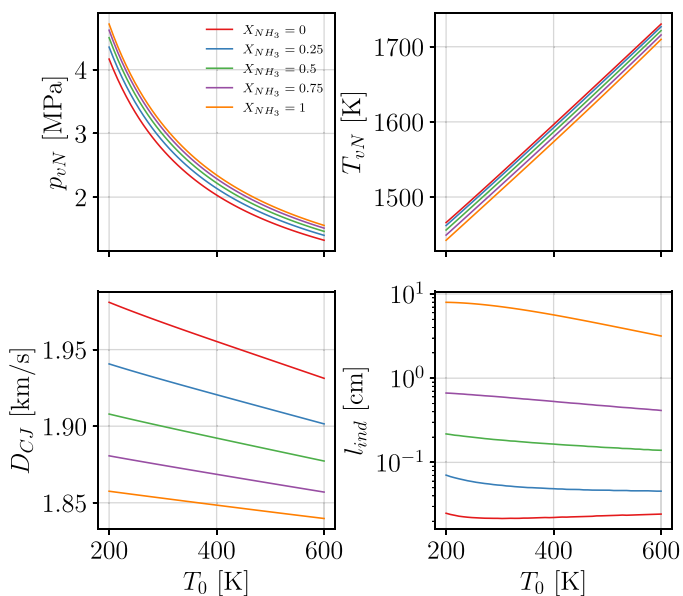

Fig. 4. Influence of initial temperature (T_0) on detonation properties for different amounts of NH$_3$. Conditions: $p_0 = 100$ kPa and $\phi = 1$.
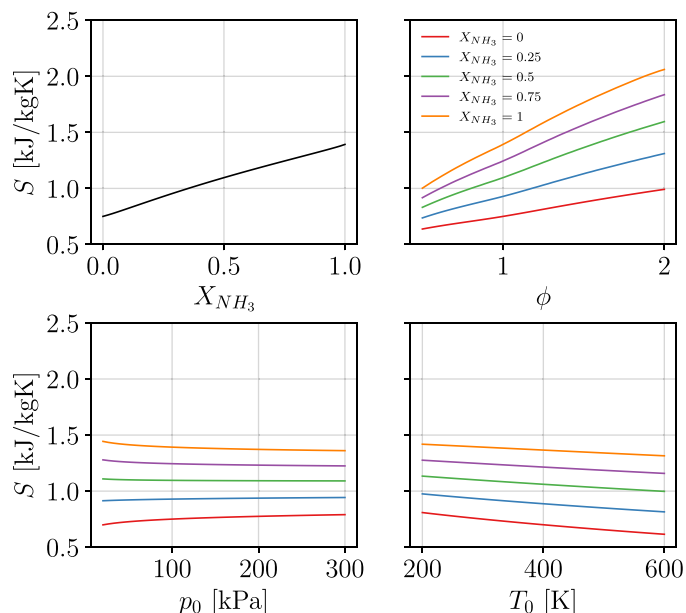

Fig. 5. Entropy production as a function of X_{NH_3}, equivalence ratio, and initial thermodynamic conditions. Conditions: $p_0 = 100$ kPa, $T_0 = 300$ K and $\phi = 1$ if not varied.

shock decreases (increases), while the detonation wave slows down when increasing the mixture temperature. For all mixtures, except for H$_2$-air, a decrease of l_{ind} is observed as T_0 is increased. For the mixture without ammonia, a more complex behavior is seen with a decrease of l_{ind} between 200 and 300 K, followed by a slight increase of l_{ind} between 300 and 600 K.

3.2.1. Entropy production

To analyze the thermodynamic efficiency of ammonia-based detonations, the total entropy production S in the detonation wave is calculated. Entropy is obtained via direct integration of the entropy rate based on the work by Chen et al. [41]. Fig. 5 shows that adding NH$_3$ to hydrogen increases the amount of entropy produced, doubling its value when comparing pure H$_2$ and pure NH$_3$. Higher entropy is usually linked with a lower thermodynamic efficiency of the process,

thus yielding lower exergy. In addition, modifying the equivalence ratio yields linear variations of entropy productions, increasing its value from 0.8 kJ/kg K for $\phi = 0.8$ to 1.35 for $\phi = 2$. Note that the higher the amount of ammonia in the mixture, the larger the slope of change of the entropy production, which demonstrates the strong influence of ϕ and of the ammonia content on entropy production. Finally, changing the initial thermodynamic conditions has a much lower substantial impact on the entropy production. Namely, increasing p_0 provokes a slight increase (decrease) of S for mixtures with less (more) than 25% of ammonia. On the other hand, higher initial temperatures T_0 yield lower entropy production for all analyzed fuel blends.

The results of a more in-depth chemical analysis of entropy production are shown in Figs. 6 and 7 for pure hydrogen and ammonia, respectively. Top sub-figures represent the temperature and thermicity ZND profiles. Sub-figures in the middle provide the total entropy formation profile and those of the top 5 reactions that contribute to this entropy production. Likewise, the top 5 reactions that contribute to the chemical heat release are included in the bottom sub-figures. It can be observed that the rate of production of entropy for pure hydrogen is much higher than for pure ammonia, with production peaks of the order of 6×10^9 and 3×10^8 W/kg K, respectively; longer reaction times yield higher final entropy values for pure ammonia. Entropy production has been related to chemical heat release, HRR, in past studies [41]. We observe here a similar behavior for pure hydrogen and ammonia, as the peaks of dS/dt and HRR happen at the same time, along with the thermicity peak and related temperature increase. Interestingly, for the pure H$_2$ case, the entropy and heat production are decoupled at the very end of the combustion process; the entropy production rate remains at a relatively high, constant level, whereas the heat production rate dramatically falls off. Such a feature does not seem to be present in the case of pure ammonia. The main reactions responsible for entropy production in the pure-H$_2$ mixture are consistent with the ones pointed out by Chen et al. [41]; reactions H + HO$_2$ $\rightleftharpoons$ 2OH, H + O$_2$(+M) $\rightleftharpoons$ HO$_2$(+M), H$_2$O + H$_2$O $\rightleftharpoons$ H + OH + H$_2$O, H$_2$ + OH $\rightleftharpoons$ H + H$_2$O dominate the entropy production. Some of the top 5 reactions involved in HRR are also very important for the S production; 2 out of 5 reactions are observed in both top 5: H + O$_2$(+M) $\rightleftharpoons$ HO$_2$(+M) and H$_2$O+H$_2$O $\rightleftharpoons$ H+OH+H$_2$O. The main reactions are completely different
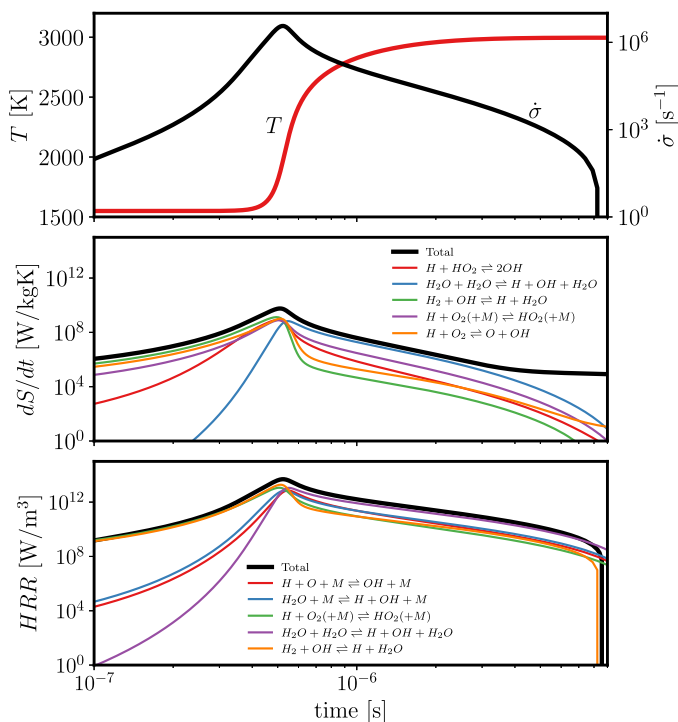
Fig. 6. *Top* - Temperature and thermicity ($\dot{\sigma}$) ZND profiles obtained for pure H_2. *Middle* - Total entropy formation and top 5 reactions that contribute to it. *Bottom* - Total HRR and top 5 reactions that contribute to it. Conditions: p_0 = 100 kPa, T_0 = 300 K and $\phi = 1$.

Fig. 7. *Top* - Temperature and thermicity ($\dot{\sigma}$) ZND profiles obtained for pure NH_3. *Middle* - Total entropy formation and top 5 reactions that contribute to it. *Bottom* - Total HRR and top 5 reactions that contribute to it. Conditions: p_0 = 100 kPa, T_0 = 300 K and $\phi = 1$.

when comparing the pure-hydrogen and the pure-ammonia cases. This is not unexpected since diverse chemical paths are activated depending on the specificity of the fuel or fuel blend. For instance, reactions including nitrogen-based compounds such as NH_2, NO and N_2O are the main species involved in entropy production for pure ammonia. The two fuels only share the reaction $H + O_2 \rightleftharpoons O + OH$ in their top 5 reactions for entropy production. Concerning heat production, we note that the two reactions $NH_3 + OH \rightleftharpoons H_2O + NH_2$ and $NNH + O_2 \rightleftharpoons HO_2 + N_2$ were also identified as important for HRR by Weng et al. [4] in their study of detonation in ammonia-based mixtures. For pure ammonia, three reactions are shared in the top 5 for entropy and heat production rate: $H + N_2O \rightleftharpoons N_2 + OH$, $HO_2 + NH_2 \rightleftharpoons H_2NO + OH$, and $NH_2 + NO \rightleftharpoons H_2O + N_2$.

To gain further insights, Fig. 8 shows the effect of ammonia percentage on the most important reactions for entropy production. The chemical picture in terms of entropy production changes a lot depending on the mixture composition. For high ammonia amount, i.e., $X_{NH_3} \sim 0.5$, reactions of the H-O chemical system are not very important, except the chain-branching reaction $H + O_2 \rightleftharpoons O + OH$, and are replaced by those involving nitrogen-based compounds. In particular, the reaction $NH_2 + NO \rightleftharpoons H_2O + N_2$ largely dominates the entropy production for mixtures with a large content of NH_3.

3.2.2. Nitrogen oxides production

Nitrogen oxides (NOx) production is of critical importance when assessing the use of fuels for powering activities, due to its strong environmental impact. Here, it is obtained by checking the amount of NO_2, N_2O and NO in the equilibrium composition (i.e., Chapman–Jouguet state) of a specific mixture.

Results shown in Fig. 9 lead to the conclusion that the amount of NOx is strongly reduced as the amount of ammonia in the fuel blend is increased. The high influence of gas temperature on thermal NOx production explains this behavior. Moreover, NO constitutes the large majority of the NOx produced. In addition, ammonia also reduces N_2O
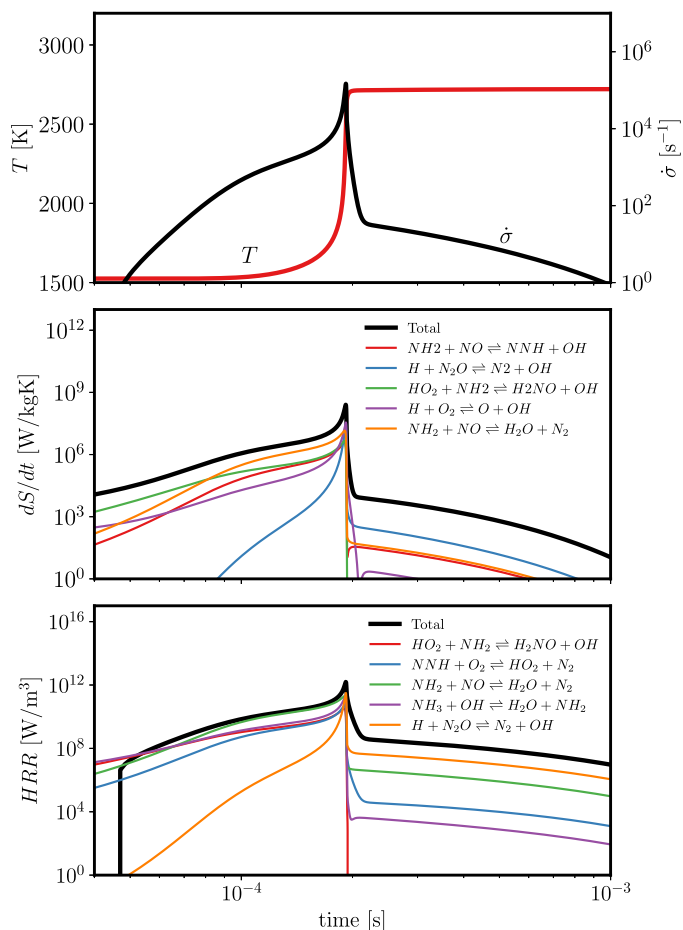
production – not shown in the figure –, a compound with a very high green-house efficiency. Indeed, previous studies [42] defend that N_2O green-house effect is 300 times higher than that of CO_2. Regardless of the amount of ammonia in the mixture, NOx production demonstrates a maximum at a lean equivalence ratio of around $\phi \sim 0.9$, which we attributed to a competition between high-temperature conditions and NOx precursors availability. Therefore, burning a leaner mixture could provide higher thermodynamic efficiency, owing to a lower entropy output, but at the expense of a higher NOx pollution. On the contrary, adding ammonia reduces the amount of NOx pollutants by a maximum factor of 2, at a cost of a higher entropy production, which almost doubles for any considered equivalence ratio. The amount of NOx produced remains almost constant regardless of the initial pressure. For example, given a constant mixture composition of X_{NH_3} = 0.25, a maximum variation of 6% between p_0 = 40 kPa and p_0 = 300 kPa is observed. Slightly stronger differences are obtained for higher ammonia presence in the mixture (e.g., maximum variation of 15%). In all cases, much lower quantities of NOx are formed as the ammonia content in the fuel increases. On the other hand, the initial temperature of the mixture has a more pronounced effect on NOx production. It almost doubles when moving from an initial temperature of 200 K to 600 K, mainly due to the highest gas temperature behind the shock and along the whole detonation structure, which promotes the production of thermal NOx. Again, the higher the amount of NH_3 on the fuel blend, the lower the amount of NOx produced.

Since the combined knowledge of entropy and NOx production could be useful to select optimum mixture composition and engine
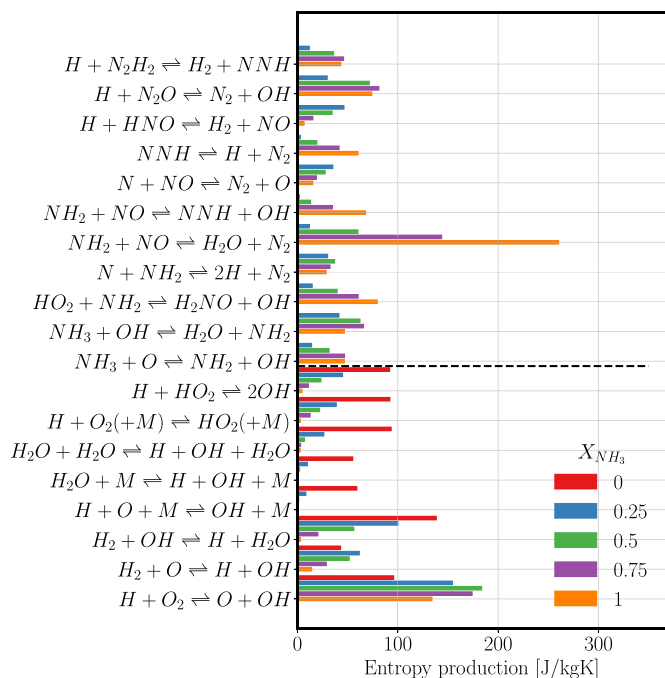
Fig. 8. Main reactions for entropy formation given a varying fuel blend composition. The horizontal black dashed line separates the reactions of the H-O-N chemical system from the reactions of the H-O system. Conditions: $p_0 = 100$ kPa, $T_0 = 300$ K and $\phi = 1$.
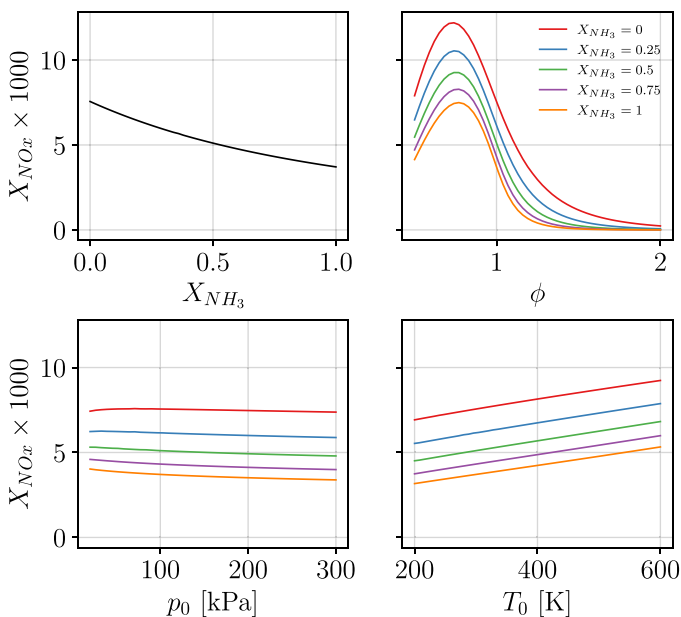

Fig. 9. NOx (NO + N_2O + NO_2) production as a function of X_{NH_3}, equivalence ratio and initial thermodynamic conditions. Conditions: $p_0 = 100$ kPa, $T_0 = 300$ K and $\phi = 1$ if not varied.

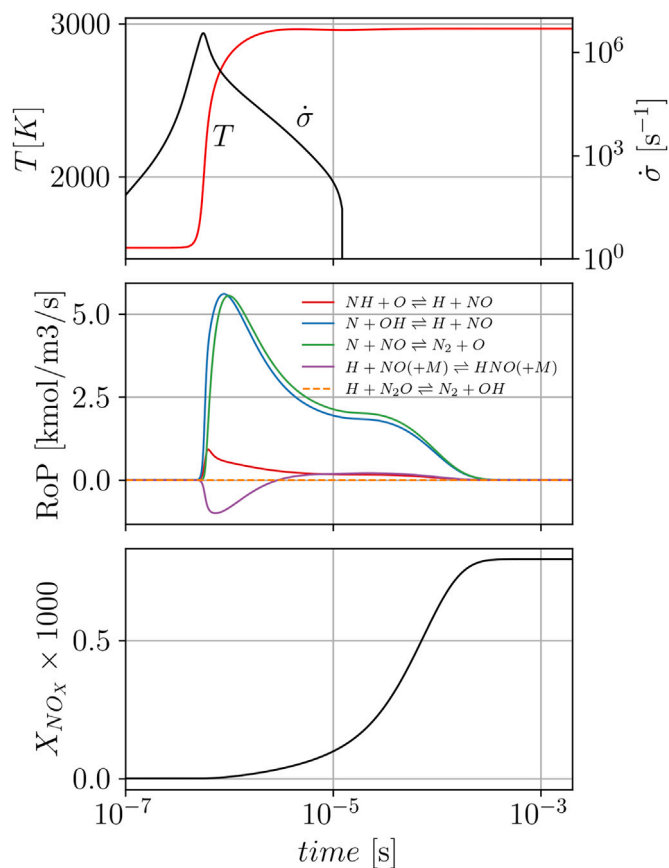**Fig. 10.** *Top* - Temperature and thermicity ($\dot{\sigma}$) ZND profiles obtained for pure H_2. *Middle* - RoP profiles of the top 5 reactions that contribute to NOx production. *Bottom* - NOx mole fraction profile. Conditions: $p_0 = 100$ kPa, $T_0 = 300$ K and $\phi = 1$.

design, we also carried out an in-depth chemical analysis of NOx production for pure hydrogen (Fig. 10) and pure ammonia (Fig. 11). Top sub-figures represent the temperature and thermicity ZND profiles. Sub-figures in the middle provide the rate of production (*RoP*) profiles of the top 5 reactions that generate/consume NOx. Moreover and for the sake of completeness, NOx mole fraction profiles are included in the bottom sub-figures. For pure hydrogen, only four reactions play a major role on NOx production, and these are related to NO kinetics. The influence of the fifth top reaction (H + N_2O ⇌ N_2 + OH) is almost

negligible, and is related to N_2O. Interestingly, the production of NOx takes place downstream the main thermicity peak for quite long times (from $t = 0.7$ μs to $t = 1$ ms), when the temperature of the gas is at its highest and thermal NOx pathways dominate NOx production. A sigmoid-shape of the NOx profile is observed. Given a pure ammonia detonation, NOx production happens at the same time as the main thermicity peak (from $t = 0.1$ ms to $t = 1$ ms). The NOx profile is very different and demonstrate a peak-shape with a strong decrease of the NOx mole fraction following the peak of thermicity. In this case, several reactions compete for producing and consuming NOx. The presence of nitrogen-based compounds, such as NH_2, activate several chemical pathways that also consume NO, whereas these reactions do not play any role for pure H_2. During a first stage before the $\dot{\sigma}$ peak, NOx are mainly generated by NH_2 + NO ⇌ H_2O + N_2 (which proceeds in the reverse direction) and HNO + O_2 ⇌ HO_2 + NO. A second stage downstream this peak yields an overall consumption of NOx. Therefore, the NOx presence at Chapman–Jouguet equilibrium condition is lower for pure ammonia, despite the fact that much higher NOx production/consumption rates are observed. For intermediate fuel blend compositions, the main reactions are included in Fig. 12. The contributions of several reactions, including HNO + O_2 ⇌ HO_2 + NO, and NH_2 + NO ⇌ H_2O + N_2, increases with the ammonia content, while the contributions of others, such as N + O_2 ⇌ NO + O, and H + HNO ⇌ H_2 + NO, demonstrate the opposite trends. It is also noted that some reactions have a more complex behavior. For examples, (i) the contributions of H + N_2O ⇌ N_2 + OH, is maximum for $X_{NH3} = 0.75$; and (ii) the contribution of H + NO(*M*) ⇌ HO_2 + NO is negative only for $X_{NH3} = 0.25$. Note the fact that even for the lowest addition of ammonia, NOx begins to be consumed; only for pure hydrogen a

higher total amount is obtained despite the lowest rates calculated. This reduced NOx production is consistent with the well known Selective Catalytic Reduction process widely used in the automotive industry to reduce NOx production by diesel engine [43].
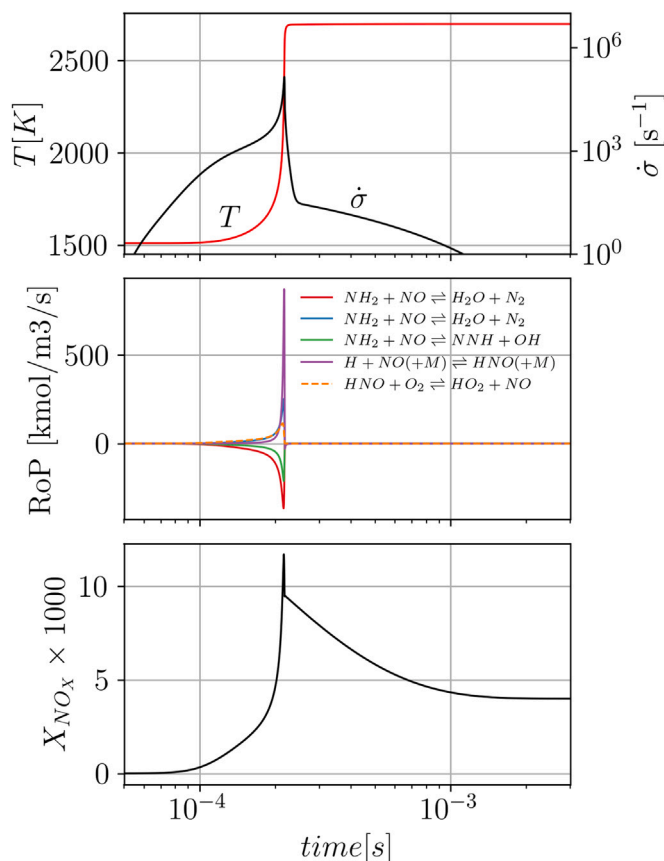

Fig. 11. *Top* - Temperature and thermicity ($\dot\sigma$) ZND profiles obtained for pure NH_3. *Middle* - RoP profiles of the top 5 reactions that contribute to NOx production. *Bottom* - NOx mole fraction profile. Conditions: $p_0 = 100$ kPa, $T_0 = 300$ K and $\phi = 1$.

Finally, it is interesting to further investigate NOx production and/or consumption downstream the sonic point/CJ condition, where a Taylor–Zeldovich [44,45] (TZ) wave expands the fluid behind a detonation until a motionless condition is reached. The properties (e.g., thermodynamic conditions, gas composition, flow speed, etc.) in the expansion wave can be obtained using a similarity solution coupled with detailed chemistry calculations. In this work we adopted the 1-γ isentropic model developed by Cooper [5]. For this analysis, we start from the equilibrium CJ conditions of the gas and perform an isentropic expansion at different rates, which depend on the distance traveled by a specific Lagrangian particle within the TZ wave. This approach provides a first-order estimation of NOx composition of the final exhaust gases expelled to the atmosphere. Note that we only studied the dynamics of NO, because it corresponds to more than 99% of the total NOx. The NO-related results within the TZ wave for pure hydrogen and ammonia are presented in Figs. 13 and 14, respectively. For most expansion rates, there is a non-linear consumption of NO during the whole process, presenting a peak at a certain position which is, in general, closer to the initial equilibrium point for longer particle path within the TZ wave. For the particles with the shortest path, a slight production of NO is observed at the very early stages of the process. After this peak of production, a similar behavior is observed for most particles with a continuous consumption. Therefore, the TZ expansion waves induces an overall reduction of the NO compared to the equilibrium CJ conditions. The features observed for pure-ammonia detonation are quite similar to those observed for pure-hydrogen detonation.
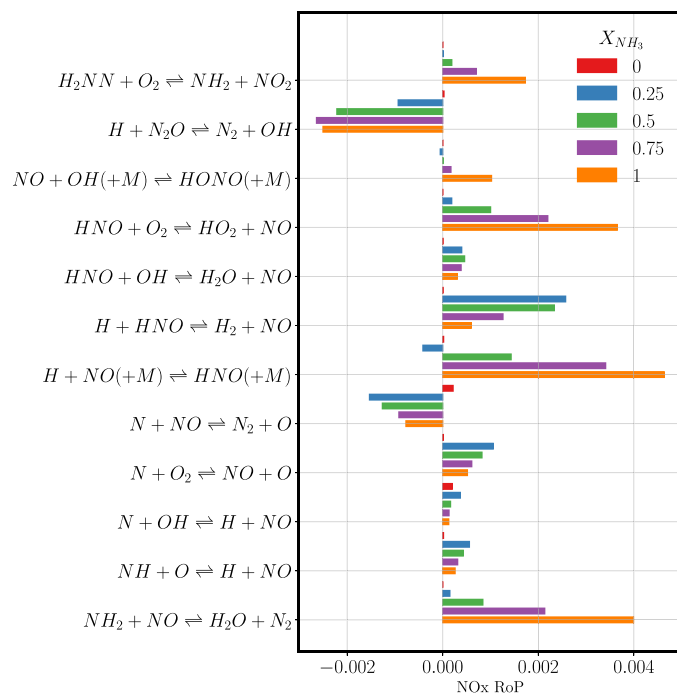

Fig. 12. Main contributing reactions to NOx formation given a varying fuel blend composition. Conditions: $p_0 = 100$ kPa, $T_0 = 300$ K and $\phi = 1$.
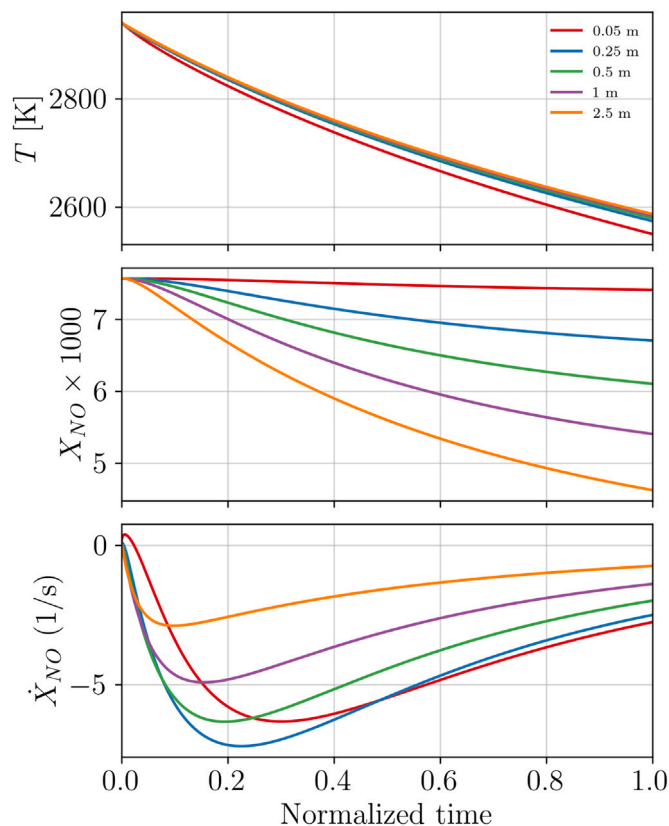

Fig. 13. Taylor–Zeldovich expansion wave analysis for pure hydrogen, starting from the Chapman–Jouguet equilibrium condition. *Top* - Temperature and pressure expansion profiles. *Middle* - NO mole fraction. *Bottom* - NO mole fraction creation/consumption rate. Conditions: $p_0 = 100$ kPa, $T_0 = 300$ K and $\phi = 1$.
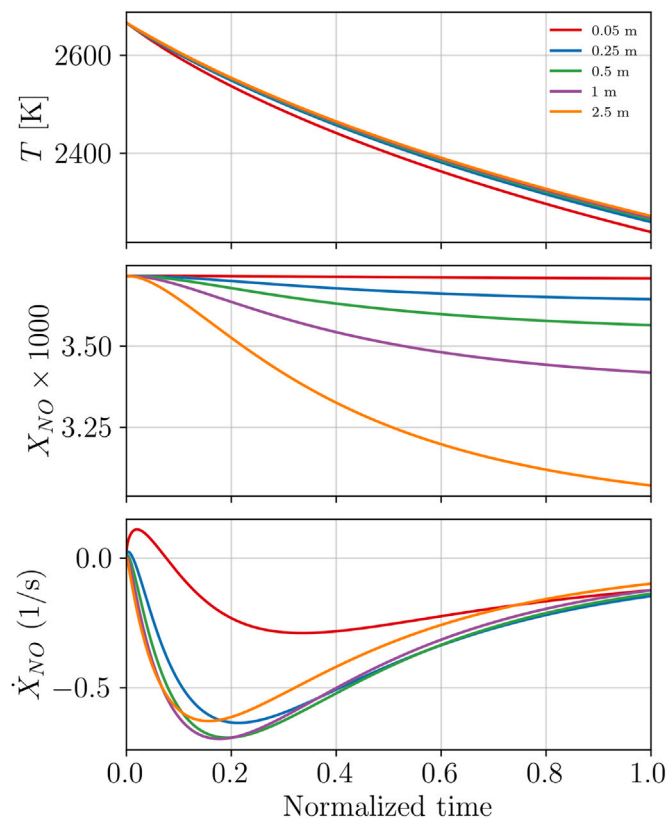
Fig. 14. Taylor–Zeldovich expansion wave analysis for pure ammonia, starting from the Chapman–Jouguet equilibrium condition. *Top* - Temperature and pressure expansion profiles. *Middle* - NO mole fraction. *Bottom* - NO mole fraction creation/consumption rate. Conditions: $p_0 = 100$ kPa, $T_0 = 300$ K and $\phi = 1$.

3.3. Curved detonations

In practical set-ups, such as rotating detonation engines (RDEs), slightly curved detonations are typically observed since the main detonation front actively interacts with an inert layer of already-burned gases and gets slightly deformed. Trying to take this effect into account and make a first assessment of the potential of H_2-NH_3 fuel blends as fuel for RDEs, we studied the influence of curvature κ on the detonation propagation ($D - \kappa$ curves), entropy generation and NOx production.
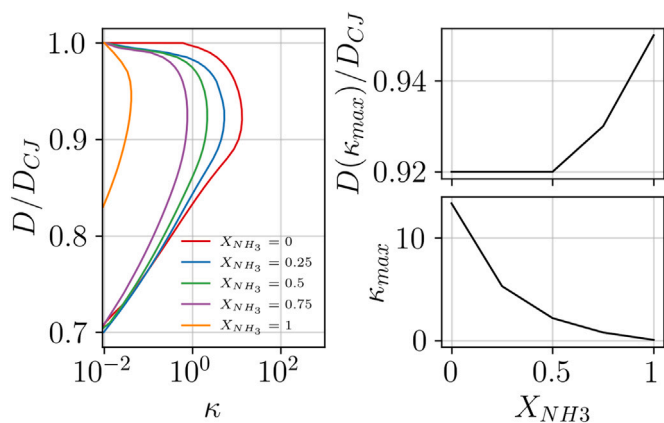

Fig. 15. $D - \kappa$ curves, maximum curvature (κ_{max}) and detonation velocity deficit at which κ_{max} is found for different H_2–NH_3 fuel blends. Conditions: $p_0 = 100$ kPa, $T_0 = 300$ K and $\phi = 1$.

Fig. 15 summarizes the curvature analysis performed. Fig. 15-left provides the $D - \kappa$ curves which relate for a given detonation deficit the curvature at which a steady solution is obtained. A good estimation of the maximum curvature (κ_{max} - Fig. 15-bottom-right) that a detonation wave can withstand is known as the critical point, i.e., the upper turnover point [25,26]. It is observed that the amount of ammonia in the blend has a dramatic effect on this parameter, reducing κ_{max} from 13 m^{-1} to 0.07 m^{-1} between pure-hydrogen and pure-ammonia cases, that is, four orders of magnitude. Therefore, ammonia detonations can only propagate in case they are almost planar, an ideal case difficult to establish in real applications. Detonations of practical interest (e.g., usable in RDEs) are found only for small-enough amounts ($X_{NH_3} \leq 0.25$) of NH_3 in the fuel blend, for which the maximum curvatures found are of the same order of magnitude as those of pure hydrogen.
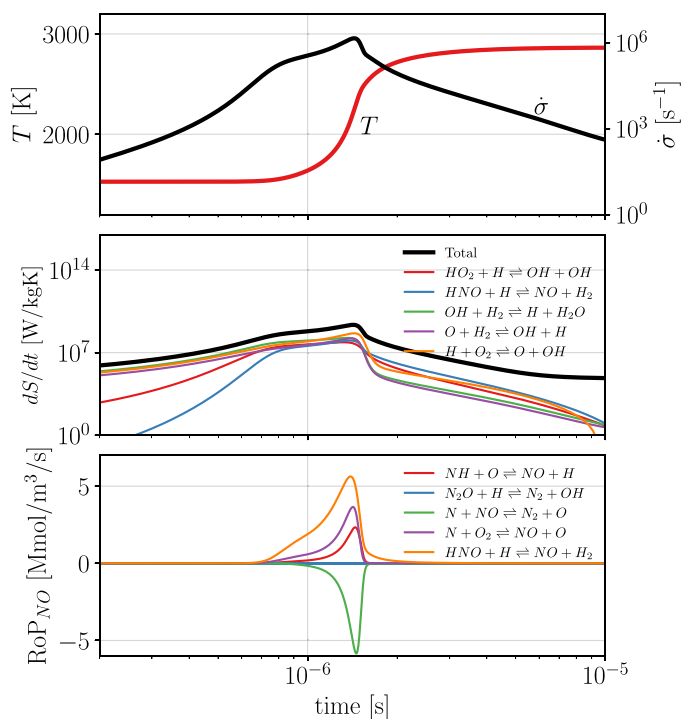

Fig. 16. *Top* - Temperature and thermicity ($\dot{\sigma}$) ideal ZND profiles obtained for a mixture with $X_{NH_3} = 0.25$. *Middle* - Total and top 5 reactions entropy production profiles. *Bottom* NO rate of production. Conditions: $p_0 = 100$ kPa, $T_0 = 300$ K and $\phi = 1$. Planar detonation with $\kappa = \kappa_{max} = 0$ m^{-1} and $D = D_{CJ} = 1967$ m/s. Conditions: $p_0 = 100$ kPa, $T_0 = 300$ K and $\phi = 1$.

Figs. 16 and 17 show the results of detailed analyses for entropy and NOx formation, performed for a constant fuel blend composition of $X_{NH_3} = 0.25$, and either an ideal, planar wave (Fig. 16) or a curved detonation with a curvature of 5.3 m^{-1}, and a detonation velocity of 1810 m/s, 92% of the ideal CJ speed (Fig. 17). These figures include the temperature and thermicity profiles, the entropy generation and NO rate of production in the top, middle and bottom sub-figures, respectively. Curved detonations happen to be slower due to the loss induced by curvature κ. Therefore, the shock is weaker, yielding less extreme von Neumann thermodynamic conditions, which slows down the chemical reaction, widens the reaction zone of the detonation (from 0.7 to 6 µs), and provokes a smoother heat deposition to the gas. The main entropy production is taking place around the thermicity peaks for both ideal and curved detonations. Faster entropy production is observed for the curved (slower) detonation than for the planar one. Regarding the top 5 reactions dominating the entropy generation, there is almost no variation. Four of the five reactions are shared by the ideal and curved detonations, but at different positions. Only HNO + H ⇌

$NO + H_2$ is replaced by $H + O_2(+M) \rightleftharpoons HO_2(+M)$ when analyzing the entropy production at the detonation's maximum sustainable curvature. Note that these reactions are top 2 and 1, respectively, showing a very important contribution to entropy production. NO production increases a lot for curved detonations, more than doubling the CJ equilibrium mole fraction from 0.6 to 1.4%, despite demonstrating a lower RoP. A key factor for NO generation is the residence time. It requires adequate thermodynamic conditions (mostly high temperature for thermal NOx) for extended periods of time. Such overall conditions are favored for curved detonation. On the other hand, the chemical pathways do not change a lot between planar and curved detonations, sharing 4/5 of the top 5 reactions as already noted for entropy production. Finally, a TZ expansion analysis was carried out from the equilibrium conditions at the sonic point for both an ideal and curved detonation with $X_{NH_3} = 0.25$, see Fig. 18. As shown for pure ammonia, the amount of NO present in the mixture always reduces regardless of the expansion rate. No major differences are found on the NO profiles, aside from the initial value which differs between ideal and curved detonations.
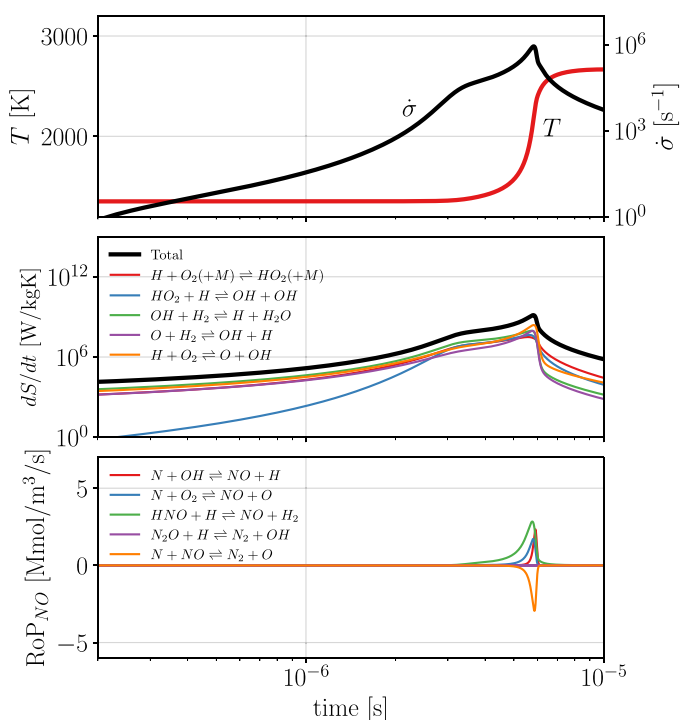

Fig. 17. *Top* - Temperature and thermicity ($\dot{\sigma}$) curved ZND profiles obtained for a mixture with $X_{NH_3} = 0.25$. *Middle* - Total and top 5 reactions entropy production profiles. *Bottom* NO rate of production. Curved detonation with $\kappa = \kappa_{max} = 5.3$ m^{-1} and $D = 0.92 D_{CJ} = 1810$ m/s. Conditions: $p_0 = 100$ kPa, $T_0 = 300$ K and $\phi = 1$.

4. Conclusion

Detonations of ammonia/hydrogen fuel blends are exhaustively analyzed in this work. Two main conclusions can be extracted from the ideal ZND chemical analysis: (i) ammonia increases the total entropy production, thus reducing the exergy efficiency of the detonation; (ii) ammonia reduces NOx production because it reduce the combustion temperature and it activates several reaction paths through which NO is consumed in the process.

In addition, to assess the potential of these blends as fuels for RDEs, curvature was included in the detonation formulation. Results show that ammonia has a dramatic effect on $D - \kappa$ curves; for a detonation in a pure-ammonia mixture, only a very small curvature would quench the detonation wave. Therefore, only slight quantities of ammonia (up to $X_{NH_3} \leq 0.25$) in the fuel blend could be used for practical applications and work in future RDEs.
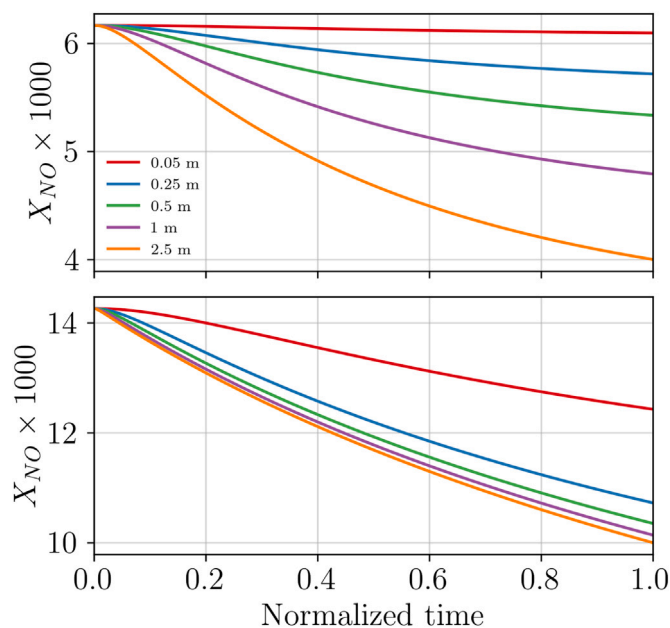

Fig. 18. Taylor Zeldovich expansion analysis for pure hydrogen from the Chapman–Jouguet equilibrium condition. *Top* - Planar detonation with $\kappa = \kappa_{max} = 0$ m^{-1} and $D = D_{CJ} = 1967$ m/s. Conditions: $p_0 = 100$ kPa, $T_0 = 300$ K and $\phi = 1$. *Bottom* - Curved detonation with $\kappa = \kappa_{max} = 5.3$ m^{-1} and $D = 0.92 D_{CJ} = 1810$ m/s. Conditions: $p_0 = 100$ kPa, $T_0 = 300$ K and $\phi = 1$.

The present results could be useful to select which range of mixture compositions could provide the best compromise between engine performance, low entropy production, and low pollutant emissions. Future efforts will be directed towards the simulation of detonation waves of low-ammonia/hydrogen detonations interacting with inert layers to obtain a better assessment of these mixtures capabilities (critical heights and/or quenching limits) for future RDE applications.

CRediT authorship contribution statement

Fernando Veiga-López: Writing – review & editing, Writing – original draft, Visualization, Validation, Software, Investigation, Formal analysis, Data curation, Conceptualization. **Rémy Mével:** Writing – review & editing, Writing – original draft, Investigation, Conceptualization.

Declaration of competing interest

The authors declare that they have no known competing financial interests or personal relationships that could have appeared to influence the work reported in this paper.

Data availability

Data will be made available on request.

References

[1] Masson-Delmotte V, Zhai P, Pirani A, Connors S, Péan C, Berger S, Caud N, Chen Y, Goldfarb L, Gomis M, Huang M, Leitzell K, Lonnoy E, Matthews J, Maycock T, Waterfield T, Yelekci O, Yu R, Zhou B. IPCC, 2021: Climate change 2021: The physical science basis. Contribution of working group I to the sixth assessment report of the intergovernmental panel on climate change. Tech. rep., Intergovernmental Panel on Climate Change; 2021.

[2] Elishav O, Mosevitzky Lis B, Miller E, Arent D, Valera-Medina A, Grinberg Dana A, Shter G, Grader G. Progress and prospective of nitrogen-based alternative fuels. Chem Rev 2020;120(12):5352–436.

[3] Valera-Medina A, Xiao H, Owen-Jones M, David W, Bowen P. Ammonia for power. Prog Energy Combust Sci 2018;69:63–102.

[4] Weng Z, Mével R, Chaumeix N. Detonation in Ammonia-oxygen and ammonia-nitrous oxide mixtures. Combust Flame 2023;251:# 112680.

[5] Cooper MA. Impulse generation by detonation tubes (Ph.D. thesis), California Institute of Technology; 2004, p. 268.

[6] Wintenberger E. Application of steady and unsteady detonation waves to propulsion (Ph.D. thesis), California Institute of Technology; 2004, p. 334.

[7] Ma J, Luan M, Xia Z, Wang J, Zhang S, Yao S, Wang B. Recent progress, development trends, and consideration of continuous detonation engines. AIAA J 2020;58(12):4976–5035.

[8] Zhou R, Wu D, Wang J. Progress of continuously rotating detonation engines. Chin J Aeronaut 2016;29(1):15–29.

[9] Eude Y. Développement d'un outil de simulation numérique des écoulements réactifs sur maillage auto-adaptatif et son application à un moteur à détonation continue (Ph.D. thesis), Université d'Orléans; 2011.

[10] Raman V, Prakash S, Gamba M. Nonidealities in rotating detonation engines. Annu Rev Fluid Mech 2023;55:639–74.

[11] Reynaud M, Virot F, Chinnayya A. A computational study of the interaction of gaseous detonations with a compressible layer. Phys Fluids 2017;29(5):# 056101.

[12] Taileb S, Melguizo-Gavilanes J, Chinnayya A. Influence of the chemical modeling on the quenching limits of gaseous detonation waves confined by an inert layer. Combust Flame 2020;218:247–59.

[13] Guirao C, Knystautas R, Lee J, Benedick W, Berman M. Hydrogen-air detonations. Symp (Int) Combust 1982;19:583–90.

[14] Pintgen F, Eckett CA, Austin JM, Shepherd JE. Direct observations of reaction zone structure in propagating detonations. Combust Flame 2003;133:211–29.

[15] Mével R, Davidenko D, Austin J, Pintgen F, Shepherd JE. Application of a laser induced fluorescence model to the numerical simulation of detonation waves in hydrogen-oxygen-diluent mixtures. Int J Hydrogen Energy 2014;39:6044–60.

[16] Mével R, Sabard J, Lei J, Chaumeix N. Fundamental combustion properties of oxygen enriched hydrogen/air mixtures relevant to safety analysis: Experimental and simulation study. Int J Hydrogen Energy 2016;41:6905–16.

[17] Shi L, Shen H, Zhang P, Zhang D, Wen C. Assessment of vibrational non-equilibrium effect on detonation cell size. Combust Sci Technol 2017;189(5):841–53.

[18] Rojas Chavez S, Chatelain K, Lacoste D. Two-dimensional visualization of induction zone in hydrogen detonations. Combust Flame 2023;255:# 112905.

[19] Akbar R, Kaneshige M, Schultz E, Shepherd J. Detonations in H_2-N_2O-CH_4-NH_3-O_2-N_2 mixtures. Tech. Rep. FM-97-3, Explosion Dynamics Laboratory, California Institute of Technology; 1997, p. 202.

[20] Vasil'ev A, Vasiliev V. Ammonia: Detonation hazards, multi-structure. In: Proceedings of the European combustion meeting. Vol. 4, 2009, p. # P810057.

[21] Yu Z, Zhang H. End-gas autoignition and knocking combustion of ammonia/hydrogen/air mixtures in a confined reactor. Int J Hydrogen Energy 2022;47:8585–602.

[22] Zhu R, Fang X, Xu C, Zhao M, Zhang H, Davy M. Pulsating one-dimensional detonation in ammonia-hydrogen-air mixtures. Int J Hydrogen Energy 2022;47:21517–36.

[23] Kohama S, Tsuboi N, Ozawa K, Hayashi A. Two-dimensional detailed numerical simulation on ammonia/hydrogen/air detonation-Stability of cell structure. In: Proceedings of the International Colloquium on the Dynamics of Explosions and Reactive Systems. Vol. 29, 2023, p. # 176.

[24] Klein R, Krok J, Shepherd J. Curved quasi-steady detonations. Asymptotic analysis and detailed chemical kinetics. Tech. Rep. FM95-04, GALCIT; 1995.

[25] Veiga-Lopez F, Weng Z, Mevel R, Melguizo-Gavilanes J. Influence of low-temperature chemistry on steady detonations with curvature losses. Proc Combust Inst 2023;39:2925–33.

[26] Weng Z, Veiga-López F, Melguizo-Gavilanes J, Mével R. Effect of ozone addition on curved detonations. Combust Flame 2023;247:# 112479.

[27] Xiao Q, Weng C. Unified dynamics of hydrogen-oxygen-diluent detonations in narrow confinements. Fuel 2023;334:# 126661.

[28] Xiao Q. On the geometrical scaling of hydrocarbon detonation dynamics. Combust Flame 2023;251:# 112714.

[29] Klein R. Analysis of accelerating detonation using large activation energy asymptotics. J Phys IV 1995;5(C4):C4–443.

[30] Yao J, Stewart D. On the normal shock velocity-curvature relationship for materials with large activation energy. Combust Flame 1995;100:519–28.

[31] He L, Clavin P. On the direct initiation of gaseous detonations by an energy source. J Fluid Mech 1994;277:227–48.

[32] Radulescu M, Borzou B. Dynamics of detonations with a constant mean flow divergence. J Fluid Mech 2018;845:346–77.

[33] Chao J, Ng H, Lee J. Detonability limits in thin annular channels. Proc Combust Inst 2009;32(2):2349–54.

[34] Shi X, Crane J, Wang H. Detonation and its limit in small tubes with ozone sensitization. Proc Combust Inst 2021;38(3):3547–54.

[35] Fernández-Tarrazo E, Gómez-Miguel R, Sánchez-Sanz M. Minimum ignition energy of hydrogen–ammonia blends in air. Fuel 2023;337:# 127128.

[36] Otomo J, Koshi M, Mitsumori T, Iwasaki H, Yamada K. Chemical kinetic modeling of ammonia oxidation with improved reaction mechanism for ammonia/air and ammonia/hydrogen/air combustion. Int J Hydrogen Energy 2018;43(5):3004–14.

[37] Dorofeev S, Sidorov V, Dvoinishnikov A. Deflagration to detonation transition in large confined volume of lean hydrogen-air mixtures. Combust Flame 1996;104:95–110.

[38] Oran E, Gamezo V, Zipf RK. Large-scale experiments and absolute detonability of methane/air mixtures. Combust Sci Technol 2015;187:324–41.

[39] Chen D, Li J, Li X, Deng L, He Z, Huang H, Kobayashi N. Study on combustion characteristics of hydrogen addition on ammonia flame at a porous burner. Energy 2023;263:# 125613.

[40] Lee J, Kim J, Park J, Kwon O. Studies on properties of laminar premixed hydrogen-added ammonia/air flames for hydrogen production. Int J Hydrogen Energy 2010;35(3):1054–64.

[41] Chen Z, Weng Z, Mével R. Entropy and nitrogen oxides production in steady detonation wave propagating in hydrogen-air mixtures. Int J Hydrogen Energy 2024;51:961–76.

[42] Richardson D, Felgate H, Watmough N, Thomson A, Baggs E. Mitigating release of the potent greenhouse gas N_2O from the nitrogen cycle–could enzymic regulation hold the key? Trends Biotechnol 2009;27(7):388–97.

[43] Maizak D, Wilberforce T, Olabi A. DeNOx removal techniques for automotive applications - A review. Environ Adv 2020;2:# 100021.

[44] Taylor GI. The dynamics of the combustion products behind plane and spherical detonation fronts in explosives. Proc R Soc Lond Ser A Math Phys Sci 1950;200(1061):235–47.

[45] Zel'dovich YB, Kompaneets A. Detonation theory. Moscow: Gostekhizdat; 1955.